The Astrophysical Journal, 844:170 (11pp), 2017 August 1 https://doi.org/10.3847/1538-4357/aa7d07

Supermassive Black Holes as the Regulators of Star Formation in Central Galaxies

Bryan A. Terrazas[1], Eric F. Bell[1], Joanna Woo[2], and Bruno M. B. Henriques[2,3]
[1] Department of Astronomy, University of Michigan, Ann Arbor, MI 48109, USA
[2] Department of Physics, Institute for Astronomy, ETH Zurich, 8093 Zurich, Switzerland
[3] Max-Planck-Institut für Astrophysik, D-85741 Garching, Germany
Received 2017 April 17; revised 2017 June 20; accepted 2017 June 30; published 2017 August 3

Abstract

We present the relationship between the black hole mass, stellar mass, and star formation rate (SFR) of a diverse group of 91 galaxies with dynamically measured black hole masses. For our sample of galaxies with a variety of morphologies and other galactic properties, we find that the specific SFR is a smoothly decreasing function of the ratio between black hole mass and stellar mass, or what we call the specific black hole mass. In order to explain this relation, we propose a physical framework where the gradual suppression of a galaxy's star formation activity results from the adjustment to an increase in specific black hole mass, and accordingly, an increase in the amount of heating. From this framework, it follows that at least some galaxies with intermediate specific black hole masses are in a steady state of partial quiescence with intermediate specific SFRs, implying that both transitioning and steady-state galaxies live within this region that is known as the "green valley." With respect to galaxy formation models, our results present an important diagnostic with which to test various prescriptions of black hole feedback and its effects on star formation activity.

Key words: galaxies: evolution – galaxies: general – galaxies: star formation

1. Introduction

Large-scale galaxy surveys have made it clear that there has been a pronounced growth in the number of galaxies that host little to no star formation (Bell et al. 2004; Brown et al. 2007; Faber et al. 2007; Ilbert et al. 2013; Muzzin et al. 2013; Tomczak et al. 2014; Mortlock et al. 2015), reflecting the overall declining cosmic star formation rate (SFR) observed in the universe since $z = 2$ (see Madau & Dickinson 2014 for a review). In an effort to understand how the quiescent population grows, these observational studies have used color–magnitude diagrams to split galaxies into a blue cloud and red sequence. Traditionally, the gap or "green valley" between these two populations has been interpreted as evidence that galaxies undergo a rapid transition from star-forming to completely quiescent, forming a sparsely populated region in this parameter space (Baldry et al. 2004; Bell et al. 2004; Faber et al. 2007; Taylor et al. 2015). However, more recent studies have proposed various quenching timescales (Martin et al. 2007; Schawinski et al. 2014; Barro et al. 2015; Woo et al. 2015), where galaxies that quench slowly may account for a large portion of the green valley population. As such, understanding the physical mechanism(s) of how individual galaxies transform and traverse the "green valley" in order to produce the growth in quiescent population has been a major topic of research in extragalactic astrophysics.

Star formation requires gas cooling down to a cold molecular form before clumps and cores begin to form systems of stellar nurseries. Therefore, the physical mechanism producing quiescence must somehow either stop gas from cooling to this form or eject the gas completely for extended periods of time. In this paper, we focus on the physics behind quiescence in central galaxies, or those at the centers of their dark matter halos, since satellite galaxies undergo unique processes that are specific to systems located well within the hot gaseous atmospheres of other galaxies.

A multitude of possible mechanisms affecting central galaxies have been proposed: stellar and supernovae Ia feedback (White & Rees 1978; Dekel & Silk 1986; White & Frenk 1991; Hopkins et al. 2012), halo-mass quenching (Cattaneo et al. 2006; Dekel & Birnboim 2006; Birnboim et al. 2007; Dekel et al. 2009; Gabor & Davé 2015), morphological quenching (Kormendy & Kennicutt 2004; Martig et al. 2009; Cisternas et al. 2011), stellar mass quenching (Peng et al. 2010), gravitational heating (Johansson et al. 2009), and varying forms of black hole feedback from active galactic nuclei (AGN, Kauffmann & Haehnelt 2000; Di Matteo et al. 2005; Croton et al. 2006; Cattaneo et al. 2009; Fabian 2012; Cicone et al. 2014).

Observationally, quiescent galaxies are more common with increasing stellar mass, and tend to host massive bulges, concentrated central stellar surface densities, concentrated light profiles, higher central velocity dispersions, and more massive dark matter halos (Kauffmann et al. 2003; Franx et al. 2008; Bell et al. 2012; Bluck et al. 2014; Lang et al. 2014; Woo et al. 2015; Mandelbaum et al. 2016). Many of these properties are expected to correlate closely with the central supermassive black hole mass (Kormendy & Ho 2013), lending support to the idea that black hole-driven feedback is important for producing quiescence in central galaxies.

Recently, a myriad of studies have compiled an ever-growing list of dynamically measured black hole masses (e.g., Kormendy & Ho 2013; Saglia et al. 2016; van den Bosch 2016), allowing a more direct and statistical study of how black holes and galactic properties correlate with one another. Terrazas et al. (2016b) used a combination of these compilations in order to show that quiescent galaxies have more massive black holes than star-forming galaxies at a given stellar mass. They also show that this behavior is naturally produced in models where star formation is regulated by long-lived radio-mode AGN feedback.

This paper aims at expanding their study by exploring exactly how the SFR of a galaxy correlates with its black hole mass and stellar mass, thereby probing the way in which the black hole responsible for AGN feedback affects the amount of star formation occurring in the galaxy.

We begin by presenting the galaxy data we use in our analysis (Section 2) and proceed to describe the resulting trends and correlations produced by the data (Section 3). We then discuss the physical framework we propose in order to interpret our results in the context of AGN feedback (Section 4.1). This motivates a discussion on whether galaxies that host intermediate amounts of star formation, or what we call "partially quiescent" galaxies, are truly transitioning (Section 4.2). Model results are then shown in order to compare our physical interpretation with the results from detailed simulations of galaxy formation (Section 4.3). We conclude with final remarks (Section 5).

2. Data

We adopt the sample of nearby ($z \lesssim 0.034$ or $d \lesssim 150$ Mpc) galaxies with dynamical estimates of black hole masses ($M_{\rm BH}$) from Terrazas et al. (2016b), where the base sample comes from Saglia et al. (2016) and is supplemented by van den Bosch (2016, and references therein). Our sample selects only central galaxies, identified as the brightest or only members in their association within a ~1 Mpc radius in order to focus on the physics of quiescence for galaxies at the centers of their potential wells.

We use extinction-corrected 2MASS "total" $K_{\rm s}$ apparent magnitudes (Huchra et al. 2012) to infer galaxy stellar masses (M_*), adopting a single K-band stellar $M_*/L_{\rm K}$ ratio of 0.75 and assuming an uncertainty of 0.15 dex. In order to calculate SFRs, we use far-infrared fluxes obtained by *IRAS* (Rice et al. 1988; Moshir et al. 1990; Surace et al. 2004; Serjeant & Hatziminaoglou 2009, see also corrections to Knapp et al. 1989 in NED) in conjunction with the methods to derive SFR described in Kennicutt & Evans (2012). Galaxies with no infrared detections or detections that result in $\mathrm{SFR}/M_* < 10^{-13}$ yr^{-1} are shown as upper limits. We adopt a 0.3 dex uncertainty for our SFR values (Bell 2003). We refer to Terrazas et al. (2016b) for more information on the methods for calculating galaxy properties.

Table 1 shows the data we used in our study, and Table 2 shows the data we used to infer galaxy properties from the literature.

3. Results

Figure 1 shows the sSFR–M_*, sSFR–$M_{\rm BH}$, and $M_{\rm BH}$–M_* parameter space for our sample of 91 central galaxies. These plots show three projections of a three-dimensional data cube where the color gradient in each panel represents the values of the third axis. We can see a clear correlation between sSFR, $M_{\rm BH}$, and M_*—namely, for a given M_*, quiescent galaxies have more massive $M_{\rm BH}$ than star-forming galaxies, as is shown and discussed in Terrazas et al. (2016b). However, galaxies at a given M_* can have diverse sSFRs that generally decrease with increasing $M_{\rm BH}$, as can be seen in the color gradient in the rightmost panel of Figure 1. This trend appears to be continuous in our data, motivating us to avoid classifying galaxies into two broad categories of "star-forming" and "quiescent." Thus, we choose to explicitly explore whether the sSFR distribution produces a dichotomy or instead varies more continuously as a function of other galaxy parameters.

In order to investigate this, we focus on the central panel of Figure 1 and show the sSFR as a function of $M_{\rm BH}$ separated into bins of M_* in Figure 2. We find that the sSFR is a smoothly declining function of $M_{\rm BH}$ in each M_* bin. The dotted black line is the same in all panels in order to show the similar slope of the relation at all M_* bins. There is also an offset in the relation between different M_* bins where less massive galaxies tend to have lower sSFRs at a given $M_{\rm BH}$ than more massive galaxies. We also note that while there is a wide range of sSFRs at a given M_*, the median sSFR at each M_* bin (open left-facing triangles) gradually decreases as M_* increases at $\log_{10} M_* > 10.75$, in accordance with the observation that more massive galaxies tend to be more quiescent. The galaxies detected at the two lowest M_* bins show lower median sSFRs. This is likely because these galaxies are not representative of the general galaxy population at these M_* bins, since most low-mass galaxies probably have central black holes with masses too low to be detected (Reines et al. 2013). Finally, we note that more massive galaxies tend to have more massive black holes, although the scatter is substantial, as is evident in the right panel of Figure 1.

The presence of a vertical offset for different M_* bins for the relations shown in Figure 2 hints at the fact that galaxies form a manifold in this three-dimensional space. We choose to fit the simplest three-dimensional manifold—a plane—to the sSFR–$M_{\rm BH}$–M_* distribution for our sample of galaxies using a linear ordinary least-squares analysis, excluding galaxies with sSFR upper limits from our fit. The result is described by the equation

$$\begin{aligned}\log_{10}\mathrm{sSFR} = {} & (0.80 \pm 0.18)\,\log_{10}\frac{M_*}{M_{*,\rm avg}} \\ & - (0.82 \pm 0.08)\,\log_{10}\frac{M_{\rm BH}}{M_{\rm BH,avg}} \\ & - (11.84 \pm 0.10), \end{aligned} \quad (1)$$

where we adopt bootstrap errors. We normalize M_* and $M_{\rm BH}$ by their average values for our sample, where $M_{*,\rm avg} = 1.62 \times 10^{11}\ M_\odot$ and $M_{\rm BH,avg} = 8.71 \times 10^8\ M_\odot$.

We note that the powers for M_* and $M_{\rm BH}$ are about equal. For this reason, Figure 3 shows a projection of this plane by plotting $\log_{10}$sSFR against the logarithm of the ratio between $M_{\rm BH}$ and M_*, or what we call the galaxy's specific black hole mass ($sM_{\rm BH}$). Dividing by M_* effectively reduces the M_* dependence the sSFR has on the $M_{\rm BH}$. We find that the sSFR is a smoothly decreasing function of the $sM_{\rm BH}$ for the overall population where the scatter is ~0.55 dex. Our result applies to a diversity of galaxy types, ranging from disky to spheroidal structures, and it spans a range of four orders of magnitude in sSFR, two orders of magnitude in stellar mass, and five orders of magnitude in black hole mass.

We color the data points by M_* to show two important features. First, we note that M_* and sSFR correlate poorly with one another compared to the correlation between $sM_{\rm BH}$ and sSFR. In other words, galaxies with similar M_* can be found anywhere along the relation, with any sSFR value, since they can have a wide variety of $sM_{\rm BH}$ values. Second, while this first point is true, more massive galaxies tend to preferentially have higher $sM_{\rm BH}$ and lower sSFRs, while the opposite is true for less massive galaxies. This reflects the general trend that more massive galaxies tend to host less star formation, and this might indicate the source of scatter in sSFR at a given M_*.

Table 1
Derived Values and Black Hole Masses

(1) Name	(2) M_* ($\log_{10} M_\odot$)	(3) SFR ($\log_{10} M_\odot$ yr^{-1})	(4) $M_{\rm BH}$ ($\log_{10} M_\odot$)	(5) $M_{\rm BH}$ Error ($\log_{10} M_\odot$)	(6) Method	(7) Ref
Centaurus A	10.904	0.213	7.755	0.084	star	1
Circinus	10.200	−0.010	6.057	0.105	maser	1
IC 1459	11.381	−0.611	9.394	0.079	star	1
IC 4296	11.567	−0.753	9.114	0.073	gas	1
M31	10.731	−0.519	8.155	0.161	star	1
M66	10.840	0.536	6.929	0.048	star	1
M81	10.764	−0.356	7.813	0.129	star, gas	1
M87	11.519	−1.335	9.789	0.031	star	1
NGC 0307	10.772	−0.567*	8.602	0.060	star	1
NGC 0524	11.086	−0.559	8.938	0.053	star	1
NGC 0821	10.779	−1.189	8.217	0.210	star	1
NGC 1023	10.756	−0.730*	7.616	0.055	star	1
NGC 1068	11.271	1.304	6.924	0.245	maser	1
NGC 1194	10.806	0.194	7.850	0.051	maser	1
NGC 1316	11.594	−0.187	8.176	0.254	star	1
NGC 1332	11.060	−0.739	9.161	0.076	star	1
NGC 1398	11.375	−0.067	8.033	0.083	star	1
NGC 1399	11.297	−1.513	8.945	0.306	star	1
NGC 1407	11.495	−1.110	9.653	0.079	star	1
NGC 1550	11.100	−0.588*	9.568	0.067	star	1
NGC 2273	10.731	0.416	6.935	0.036	maser	1
NGC 2549	10.172	−1.706	7.161	0.367	star	1
NGC 2787	10.022	−1.750	7.610	0.088	gas	1
NGC 2960	10.925	0.265	7.033	0.049	maser	1
NGC 2974	11.354	−0.791	8.230	0.091	star	1
NGC 3079	10.683	0.782	6.398	0.049	maser	1
NGC 3115	10.789	−2.146	8.953	0.095	star	1
NGC 3227	10.882	0.398	7.322	0.232	star	1
NGC 3245	10.698	−0.306	8.378	0.114	gas	1
NGC 3368	10.689	−0.222	6.875	0.076	star	1
NGC 3393	10.943	0.439	7.196	0.330	maser	1
NGC 3414	10.797	−1.047	8.400	0.071	star	1
NGC 3585	11.126	−1.391	8.517	0.127	star	1
NGC 3607	11.097	−0.319	8.137	0.157	star	1
NGC 3842	11.577	0.382	9.959	0.139	star	1
NGC 3923	11.234	−1.766*	9.449	0.115	star	1
NGC 3998	10.548	−1.210	8.927	0.052	star	1
NGC 4151	10.837	0.051	7.813	0.076	star	1
NGC 4258	10.721	−0.080	7.577	0.030	maser	1
NGC 4261	11.427	−1.359	8.723	0.097	gas	1
NGC 4291	10.664	−1.193*	8.990	0.155	star	1
NGC 4472	11.663	−1.337*	9.398	0.037	star	1
NGC 4594	11.322	−0.412	8.823	0.045	star	1
NGC 4697	10.832	−1.349	8.305	0.112	star	1
NGC 4699	11.140	0.125	8.246	0.052	star	1
NGC 4736	10.539	−0.061	6.831	0.123	star	1
NGC 4826	10.774	0.009	6.193	0.131	star	1
NGC 4889	11.836	0.034*	10.320	0.437	star	1
NGC 5018	11.319	−0.080	8.021	0.078	star	1
NGC 5077	11.070	−0.976	8.932	0.268	gas	1
NGC 5328	11.410	−0.390*	9.672	0.158	star	1
NGC 5419	11.686	−0.767	9.860	0.144	star	1
NGC 5846	11.204	−1.453	9.041	0.058	star	1
NGC 6086	11.475	0.310*	9.573	0.167	star	1
NGC 6251	11.641	0.707*	8.788	0.155	gas	1
NGC 7052	11.450	0.176	8.598	0.230	gas	1
NGC 7457	10.107	−1.869	6.954	0.302	star	1
NGC 7582	10.953	1.066	7.741	0.205	gas	1
NGC 7619	11.395	−0.353	9.398	0.108	star	1
NGC 7768	11.576	0.151*	9.127	0.181	star	1
UGC 3789	10.775	0.351	6.985	0.085	maser	1
3C120	11.448	1.155	7.730	0.150	RM	2

Table 1
(Continued)

(1) Name	(2) M_* ($\log_{10} M_\odot$)	(3) SFR ($\log_{10} M_\odot$ yr^{-1})	(4) M_{BH} ($\log_{10} M_\odot$)	(5) M_{BH} Error ($\log_{10} M_\odot$)	(6) Method	(7) Ref
Ark 120	11.555	0.800	8.050	0.170	RM	2
IC 1481	10.843	0.689	7.150	0.130	maser	2
Mrk 110	10.822	0.257	7.280	0.210	RM	2
Mrk 279	11.384	1.035	7.400	0.230	RM	2
Mrk 290	10.687	−0.029	7.260	0.170	RM	2
Mrk 335	11.251	0.403	7.210	0.160	RM	2
Mrk 509	11.525	1.108	8.030	0.150	RM	2
Mrk 590	11.478	0.610	7.550	0.180	RM	2
Mrk 79	11.230	0.820	7.580	0.230	RM	2
Mrk 817	11.304	1.216	7.570	0.180	RM	2
NGC 1600	12.175	−0.077	10.230	0.040	star	2
NGC 3516	10.942	0.066	7.370	0.160	RM	2
NGC 3783	10.981	0.434	7.360	0.190	RM	2
NGC 4253	10.737	0.734	6.800	0.170	RM	2
NGC 4593	11.164	0.381	6.860	0.210	RM	2
NGC 5273	10.099	−0.961	6.610	0.270	RM	2
NGC 5548	11.165	0.445	7.700	0.130	RM	2
NGC 5765b	11.209	1.434	7.660	0.030	maser	2
NGC 6814	10.843	0.286	7.020	0.170	RM	2
NGC 7469	11.011	1.434	6.940	0.160	RM	2
NGC 1097	11.009	0.766	8.140	0.090	CO	2
NGC 1275	11.646	1.109	8.980	0.200	gas	2
NGC 3665	11.194	0.246	8.760	0.090	CO	2
NGC 3706	11.361	−1.002	9.770	0.060	star	2
NGC 4303	10.955	0.674	6.510	0.740	gas	2
NGC 4742	10.226	−1.175	7.100	0.150	star	2
NGC 5495	11.392	0.963	7.080	0.300	maser	2
NGC 7332	10.656	−1.279	7.080	0.180	star	2

Notes. Columns: (1) Galaxy name; (2) stellar mass derived from 2MASS K_s apparent magnitudes, where we assume an error of 0.15 dex; (3) star formation rate derived from far-infrared measurements, where values with an asterisk indicate upper limits and where we assume an error of 0.3 dex; (4)–(5) black hole mass and error; (6) black hole mass measurement method—either stellar dynamics, CO, or gas dynamics, masers, or reverberation mapping; (7) references for black hole measurement: 1—Saglia et al. (2016); 2—van den Bosch (2016).

We note that a similar negative correlation is found in the central panel of Figure 1, where there is no dependence on M_*. We find that the scatter in sSFR at a given M_{BH} is 0.61 dex. Allowing the sSFR to be a function of both M_{BH} and M_* provides a better fit with 0.55 dex scatter—corresponding to a reduction by a fifth of the total variance in the central panel of Figure 1—and is preferred at >99.99% level of all fits of bootstrapped samples having no M_* dependence. Even so, we stress that the exact powers of M_{BH} and M_* need to be confirmed with a larger and more complete sample than is offered by current black hole data sets. We note that alternative versions of this fit, using different prescriptions for estimating SFR (e.g., including UV detections) and different selections for the central galaxy sample give similar results, with the fit parameters varying within their quoted errors.

4. Discussion

4.1. Physical Framework and Interpretation

Our main result is that the sSFR of a galaxy correlates smoothly with sM_{BH}, suggesting that the star-forming properties of a galaxy are in some way connected to the properties of the central black hole. While the amount of scatter is significant at 0.55 dex, the negative correlation in our data is clearly present. In order to make physical sense of this, we argue that the sSFR can only know about the M_{BH} and M_* if one of two scenarios occur: (1) black hole feedback, assuming it is measurable via M_{BH}, regulates the amount of star formation in the galaxy to some degree, or (2) the increase in M_{BH} and decrease in sSFR are due to a strongly correlated but separate process where there is no direct causal connection between the two.

Recent galaxy formation models have relied on black hole-driven AGN feedback as the primary cause of quiescence (Croton et al. 2006; Sijacki et al. 2007; Guo et al. 2010; Porter et al. 2014; Vogelsberger et al. 2014; Henriques et al. 2015; Schaye et al. 2015) since no other mechanism can produce a strong enough suppression of stellar mass build-up in high-mass galaxies (Bower et al. 2006). Terrazas et al. (2016b) shows that out of the four models analyzed, only those models that use radio-mode AGN feedback to provide a continuous source of heat reproduce the observational result that quiescent and star-forming galaxies lie in distinct regions on the M_{BH}–M_* plane where quiescent galaxies have more massive black holes than star-forming galaxies; this is unlike those models that use halo-mass quenching or quasar-mode AGN feedback as the primary source of quiescence. As a result, we set up a physical framework where we focus on scenarios that causally link the M_{BH} and the sSFR of a galaxy.

Successful simulations have modeled AGN feedback in the radio mode as bubbles expanding into the circumgalactic

Table 2
Fluxes and Distances from the Literature

(1) Name	(2) Distance (Mpc)	(3) Distance Error (Mpc)	(4) K_s	(5) *IRAS* 12μ (Jy)	(6) *IRAS* 25μ (Jy)	(7) *IRAS* 60μ (Jy)	(8) *IRAS* 100μ (Jy)	(9) MIPS 70μ (Jy)	(10) *IRAS* Ref	(11) MIPS Ref
Centaurus A	3.620	0.200	3.490	23.030	30.740	217.570	501.200	⋯	1	⋯
Circinus	2.820	0.470	4.710	18.800	68.440	248.700	315.850	⋯	5	⋯
IC1459	28.920	3.739	6.810	0.170	0.320	0.510	1.180	0.542	2	1
IC4296	49.200	3.628	7.500	⋯	⋯	0.140	0.260	0.118	2	1
M31	0.774	0.032	0.573	163.000	108.000	536.000	2928.400	1200.000	1	3
M66	10.050	1.092	5.869*	4.170	7.720	56.310	144.960	91.900	1	2
M81	3.604	0.133	3.831	5.860	5.420	44.700	174.000	85.300	1	2
M87	16.680	0.615	5.270	0.440	0.187	0.390	0.410	0.483	2	1
NGC 0307	52.800	5.736	9.641	⋯	⋯	⋯	⋯	⋯	2	⋯
NGC 0524	24.220	2.234	7.163	0.240	⋯	0.760	2.050	⋯	2	⋯
NGC 0821	23.440	1.837	7.861	⋯	⋯	⋯	0.500	⋯	2	1
NGC 1023[a]	10.810	0.797	6.238	0.240	⋯	⋯	⋯	⋯	2	1
NGC 1068	15.900	9.411	5.788	39.700	85.040	176.200	224.000	⋯	3	⋯
NGC 1194	57.980	6.299	9.758	0.266	0.512	0.770	⋯	⋯	3	⋯
NGC 1316	18.600	0.600	5.320	0.330	0.290	3.070	8.110	5.440	2	1
NGC 1332	22.300	1.851	7.050	0.100	0.110	0.510	1.810	⋯	2	⋯
NGC 1398	24.770	4.125	6.49*	0.143	0.116	1.141	8.963	⋯	3	⋯
NGC 1399	20.850	0.672	6.310	0.100	⋯	⋯	0.300	0.016	2	1
NGC 1407	28.050	3.367	6.460	0.120	⋯	0.140	0.480	⋯	2	1
NGC 1550	51.570	5.603	8.770	⋯	⋯	⋯	⋯	⋯	2	⋯
NGC 2273	29.500	1.903	8.480	0.400	1.360	6.020	10.000	⋯	3	⋯
NGC 2549	12.700	1.642	8.046	⋯	⋯	0.260	0.370	⋯	2	⋯
NGC 2787	7.450	1.241	7.263	0.080	0.100	0.600	1.180	1.017	2	1
NGC 2960	67.100	7.120	9.780	⋯	⋯	0.708	1.657	⋯	3	⋯
NGC 2974	21.500	2.381	6.236	⋯	⋯	0.420	1.900	0.682	2	1
NGC 3079	15.900	1.246	7.258	1.523	2.272	44.500	89.200	63.700	3	4
NGC 3115	9.540	0.396	5.883	0.360	0.110	0.130	⋯	0.052	2	1
NGC 3227	23.750	2.630	7.631	0.667	1.764	7.825	17.590	⋯	3	⋯
NGC 3245	21.380	1.972	7.862	0.160	0.230	2.030	3.970	⋯	2	⋯
NGC 3368	10.400	0.959	6.320	0.535	0.544	8.261	25.930	14.500	3	2
NGC 3393	49.200	8.194	9.059	0.131	0.753	2.251	3.873	⋯	3	⋯
NGC 3414	25.200	2.738	7.972	0.080	⋯	0.250	0.560	⋯	2	⋯
NGC 3585	20.510	1.702	6.703	0.120	0.210	0.160	⋯	0.080	2	1
NGC 3607	22.650	1.775	6.990	⋯	⋯	⋯	⋯	1.761	⋯	1
NGC 3842	92.200	10.638	8.840	0.090	⋯	0.360	1.490	⋯	2	⋯
NGC 3923	20.880	2.700	6.471*	0.130	⋯	⋯	⋯	0.024	2	1
NGC 3998	14.300	1.253	7.365	0.140	0.130	0.550	1.150	⋯	2	⋯
NGC 4151	20.000	2.772	7.371	1.970	4.830	6.320	7.640	⋯	3	⋯
NGC 4258	7.270	0.503	5.464	2.250	2.810	21.600	78.390	40.700	1	2
NGC 4261	32.360	2.835	6.940	0.180	0.090	0.080	0.150	0.127	2	1
NGC 4291	26.580	3.931	8.420	⋯	⋯	⋯	⋯	⋯	2	1
NGC 4472	17.140	0.592	4.970	0.200	⋯	⋯	⋯	0.061	2	1
NGC 4594	9.870	0.819	4.625	0.740	0.500	4.260	22.900	7.310	1	2
NGC 4697	12.540	0.404	6.370	0.290	⋯	0.460	1.240	0.618	2	1
NGC 4699	18.900	2.053	6.489	0.383	0.340	4.979	19.020	⋯	3	⋯
NGC 4736	5.000	0.786	5.106	4.770	6.830	62.410	135.340	101.000	1	2
NGC 4826	7.270	1.177	5.330	1.710	2.000	33.860	77.380	52.900	1	2
NGC 4889	102.000	5.169	8.410	⋯	⋯	⋯	⋯	⋯	2	⋯
NGC 5018	40.550	4.867	7.700	0.200	⋯	0.950	1.860	1.174	2	1
NGC 5077	38.700	8.442	8.220	⋯	⋯	⋯	⋯	0.133	⋯	1
NGC 5328	64.100	6.964	8.467	⋯	⋯	⋯	⋯	⋯	2	⋯
NGC 5419	56.200	6.106	7.492*	⋯	⋯	⋯	0.230	⋯	2	1
NGC 5846	24.900	2.297	6.929	⋯	⋯	⋯	⋯	0.107	2	1
NGC 6086	138.000	11.452	9.970	⋯	⋯	⋯	⋯	⋯	2	⋯
NGC 6251[a]	108.400	8.996	9.030	⋯	0.100	⋯	⋯	⋯	2	⋯
NGC 7052	70.400	8.449	8.570	0.050	⋯	0.450	1.420	⋯	2	⋯
NGC 7457	12.530	1.214	8.179	⋯	⋯	0.110	0.450	⋯	2	1
NGC 7582	22.300	9.845	7.316	1.620	6.436	49.100	72.920	⋯	3	⋯
NGC 7619	51.520	7.380	8.030	⋯	⋯	⋯	0.710	⋯	2	1
NGC 7768	116.000	27.495	9.340	⋯	⋯	⋯	⋯	⋯	2[b]	⋯
UGC 3789	49.900	5.421	9.510	0.111	0.329	1.669	3.377	⋯	3	⋯
3C120	141.400	14.100	10.089	0.286	0.635	1.283	2.786	⋯	3	⋯

Table 2
(Continued)

(1) Name	(2) Distance (Mpc)	(3) Distance Error (Mpc)	(4) K_s	(5) *IRAS* 12μ (Jy)	(6) *IRAS* 25μ (Jy)	(7) *IRAS* 60μ (Jy)	(8) *IRAS* 100μ (Jy)	(9) MIPS 70μ (Jy)	(10) *IRAS* Ref	(11) MIPS Ref
Ark 120	140.100	14.000	9.803	0.319	0.410	0.643	1.084	⋯	3	⋯
IC 1481	89.900	9.000	10.62*	⋯	0.275	1.410	1.510	⋯	3	⋯
Mrk 110	151.100	15.100	11.8*	⋯	⋯	0.131	⋯	⋯	6	⋯
Mrk 279	130.400	13.000	10.073	⋯	⋯	1.255	2.200	⋯	3	⋯
Mrk 290	126.700	⋯	11.754*	⋯	⋯	0.140	0.136	0.172	6	5
Mrk 335	110.500	⋯	10.047	0.302	0.378	0.343	⋯	⋯	3	⋯
Mrk 509	147.300	14.700	9.985	0.316	0.702	1.364	1.521	1.440	3	5
Mrk 590	113.000	11.300	9.527	0.192	0.221	0.489	1.457	⋯	3	⋯
Mrk 79	95.000	9.500	9.772	0.306	0.763	1.503	2.363	⋯	3	⋯
Mrk 817	134.700	13.500	10.344	0.336	1.175	2.118	2.268	⋯	3	⋯
NGC 1600	126.300	11.600	8.026	⋯	⋯	0.100	0.190	⋯	2	⋯
NGC 3516	37.900	3.800	8.497	0.410	1.010	1.850	2.130	⋯	2	⋯
NGC 3783	41.700	4.200	8.606	0.840	2.492	3.257	4.899	⋯	3	⋯
NGC 4253	55.400	5.500	9.832	0.386	1.300	4.030	4.660	⋯	3	⋯
NGC 4593	38.500	3.900	7.976	0.344	0.809	3.052	5.947	⋯	3	⋯
NGC 5273	15.500	1.500	8.661	0.120	0.290	0.900	1.560	0.657	2	1
NGC 5548	73.600	7.400	9.380	0.401	0.769	1.073	1.614	⋯	3	⋯
NGC 5765b	126.300	12.600	10.442	0.291	0.752	3.367	5.830	⋯	3	⋯
NGC 6814	22.300	2.200	7.591	⋯	0.599	5.517	18.880	⋯	3	⋯
NGC 7469	47.700	8.100	8.823	1.348	5.789	25.870	34.900	⋯	4	⋯
NGC 1097	14.500	⋯	6.243	2.880	7.700	46.730	116.340	59.840	1	2
NGC 1275	70.000	⋯	8.068	0.950	2.830	5.760	7.500	3.990	2	6
NGC 3665	34.700	⋯	7.675	0.110	0.210	1.910	7.530	⋯	2	⋯
NGC 3706	46.000	⋯	7.869	0.080	⋯	0.070	0.220	⋯	2	1
NGC 4303	17.900	⋯	6.835	1.064	1.401	23.640	64.650	⋯	3	⋯
NGC 4742	15.700	⋯	8.371	⋯	⋯	0.450	1.150	⋯	2	⋯
NGC 5495	103.000	⋯	9.543	0.112	⋯	1.487	3.534	⋯	3	⋯
NGC 7332	21.700	⋯	7.999	0.120	⋯	0.210	0.410	⋯	2	⋯

Notes. Columns: (1) Galaxy name; (2)–(3) distances and errors taken from the same references as the black hole masses, see column 7 in Table 1; (4) extinction-corrected 2MASS "total" K_s apparent magnitudes from Huchra et al. (2012) unless the value has an asterisk, in which case these are taken from the 2MASS LGA Catalog (Jarrett et al. 2003); (5)–(8) *IRAS* 12μ, 25μ, 60μ, and 100μ flux measurements; (9) MIPS 70μ flux measurements; (10) *IRAS* measurement. References: 1—Rice et al. (1988), 2—Corrections to Knapp et al. (1989) in NED by Knapp, 3—Moshir et al. (1990), 4—Surace et al. (2004), 5—Ghosh et al. (1992), 6—Serjeant & Hatziminaoglou (2009); (11) MIPS measurement. References: 1—Temi et al. (2009), 2—Dale et al. (2009), 3—Tempel et al. (2010), 4—Engelbracht et al. (2008), 5—Shang et al. (2011), 6—Landt et al. (2010). If there is a reference but no flux measurement, this is taken to be a non-detection.

[a] The SFRs for NGC 1023 and NGC 6251 are calculated based on 12 and 25 μm detections and therefore may be contaminated by an AGN. We therefore use these detections to obtain upper limits on these galaxies' SFRs.

[b] NGC 7768 has an *IRAS* 25 μm detection, but is likely contaminated by a nearby star, therefore we omit this value since it is clearly an elliptical BCG.

medium around a galaxy in order to heat the surrounding gas, thereby cutting off the fuel needed for star formation (e.g., Croton et al. 2006; Sijacki et al. 2007). While black hole feeding likely occurs at irregular intervals depending on gas availability, bubbles formed by radio-mode AGN feedback expand into the medium long after accretion stops. In this physical scenario, the heating from the expansion of these bubbles is likely to be more or less continuous even though black hole feeding is not. Observationally, this idea is supported by the presence of long-lived X-ray cavities and "ghost" cavities from past accretion events in the intracluster medium around cluster, group, and isolated galaxies (Bîrzan et al. 2004; David et al. 2009; Gitti et al. 2010; Shin et al. 2016).

Models also show that the M_{BH} correlates with the amount of heating from AGN feedback (Sijacki et al. 2015; Terrazas et al. 2016b). In accordance with this, our observational results in Section 3 show that higher values of sM_{BH} result in correspondingly lower values of sSFR to produce a negative correlation. A possible interpretation is that the sSFR adjusts to the sM_{BH} at least at $z = 0$ to produce a smoothly declining relation between these two parameters. This adjustment must occur on short enough timescales to allow such a relation between sSFR and sM_{BH}. In other words, if either of these quantities could drastically change without allowing the other quantity to adjust, then a relation between these two parameters would not appear as clearly as it does in Figure 3.

In addition, we note that the shape of the relation is important: a smoothly declining relation may hint at the physics behind heating and cooling of gas around the galaxy. More specifically, this may mean that an intermediate sM_{BH} results in an intermediate amount of gas heating that decreases, but does not completely halt, the amount of gas cooling onto the disk to fuel star formation in the galaxy. We expand on this issue in Section 4.2, where we discuss the phenomenon of partial quiescence.

The vertical offset in the relations between sSFR and M_{BH} from low- to high-M_* bins in Figure 2 can be interpreted to mean that more massive galaxies need a more massive black hole to maintain the same degree of quiescence as less massive galaxies, since more massive galaxies have a deeper potential well, and in the absence of heating, would be forming more

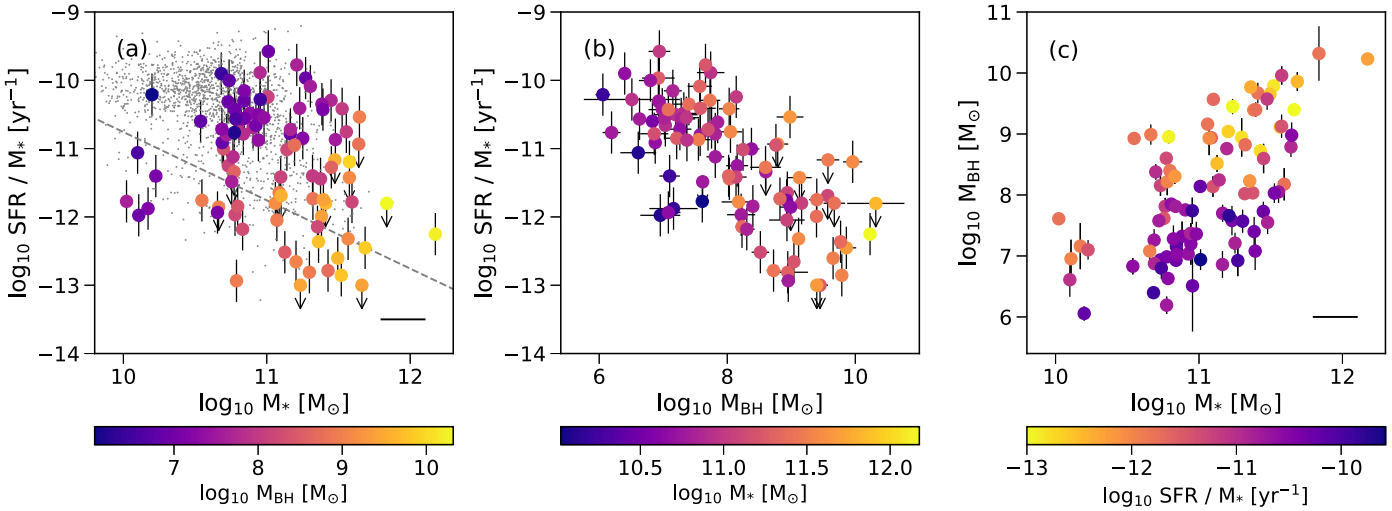

Figure 1. Projections of the three-dimensional sSFR–M_{BH}–M_* data cube: (a) sSFR as a function of M_*. The gray data points indicate a sample of local galaxies to show the star-forming main sequence. The dashed line indicates the boundary below which the sample is no longer complete; (b) sSFR as a function of M_{BH}; (c) M_{BH} as a function of M_*. Color gradients indicate the values for the axis not shown. The lines at the bottom right of (a) and (c) indicate the errors on M_*.

stars as a result of cooling and gravity. However, more massive galaxies also tend to have lower sSFRs than the less massive galaxies, in general agreement with other studies (Brinchmann et al. 2004; Salim et al. 2007). This implies that the M_{BH} of massive galaxies are significantly higher than those of less massive galaxies, resulting in the vast majority of the high-M_* galaxy population to be predominantly quiescent. In addition, the fact that we normalize both the SFR and M_{BH} by M_* tells us that reducing the dependence on the depth of the potential well—represented by M_* in this paper—gives us a similar relation across a diverse group of central galaxies with $M_* > 10^{10}\,M_\odot$.

We also note that the scatter between sSFR and M_{BH} increases in the highest M_* bin in Figure 2. This could be due to multiple factors. For one, M_* is likely an increasingly poor tracer of a galaxy's potential well at high-M_* since the M_*–M_h relation becomes substantially flatter at these mass regimes (Behroozi et al. 2010, 2013; Moster et al. 2010). Instead, obtaining a halo mass may be more effective, albeit more difficult, and may eliminate the increased scatter. In addition, low sSFR values are increasingly difficult to measure and may have less meaning with regard to the actual amount of star formation in the galaxy. Another explanation may be that more massive galaxies are probing clusters rather than groups and isolated galaxies. Black hole feedback in these systems may differ in terms of how gas heating and cooling operates (Gaspari et al. 2011).

An important assumption we have made is that M_{BH} is measuring the amount of heating energy being injected into the gas around the galaxy, while the sSFR is measuring the amount of gas cooling onto the galaxy. In the real Universe, these parameters may vary widely on a galaxy-to-galaxy basis based on the state of the gas, the star formation efficiency of the galaxy, the duty cycle and jet power of the black hole feedback and how that correlates with M_{BH}, and potentially many other factors.

4.2. Partial Quiescence

Galaxies that have low yet significant amounts of star formation in our sample are shown in the light gray band in Figure 3. Previous studies have often referred to these galaxies as transitioning or "green valley" galaxies (Balogh et al. 2004; Bell et al. 2004; Martin et al. 2007; Brammer et al. 2009; Mendez et al. 2011; Gonçalves et al. 2012; Wetzel et al. 2012; Krause et al. 2013; Pan et al. 2014), assuming they are on their way to becoming completely quiescent. Given the dearth of galaxies in this region in a color–magnitude diagram, the traditional view is that galaxies quickly move from the blue cloud to the red sequence, or, as has been interpreted, from star-forming to quiescent (e.g., Baldry et al. 2004).

A smoothly decreasing correlation between the sSFR and sM_{BH} shown in Figure 3 and described in Section 3 is perhaps unexpected given the commonly held belief that galaxies exist only briefly in this transition state. If the M_{BH} grows significantly, then in order to land on the relation in Figure 3 and agree with our observational result, the galaxy must also decrease its sSFR accordingly. Therefore, a star-forming galaxy that grows its black hole to an intermediate sM_{BH} must also decrease its sSFR to an intermediate value on timescales short enough to produce a relation between the two quantities.

We note that this framework does not require central galaxies with intermediate sSFRs to be transitioning at all. A central galaxy can stay in the "green valley" as long as it no longer grows its sM_{BH}. In this scenario, the relation between sSFR and sM_{BH} represents the amount of star formation that results from the balance between heating and cooling represented by the ratio between a galaxy's M_{BH} and M_*. If this is the case, then this framework implies that all central massive galaxies tend toward an equilibrium position defined by this relation, which determines their sSFR from their sM_{BH}, and that much of the scatter likely comes from the time it takes for the sSFR to adjust to the sM_{BH}.

As a result, the fact that the sSFR, M_{BH}, and M_* are smooth but scattered functions of each other leads us to argue that many of the partially quiescent galaxies in our sample may not be transitioning—instead, they may maintain a quasi-stable state of quiescence that correlates with their M_{BH} and M_*.

One possible example of this in our sample is M31, labeled in Figure 3. M31 is not undergoing any drastic event that suggests it is quenching and heading toward a completely quiescent state. Yet many studies have shown that M31 has a lower sSFR (Kang et al. 2009; Ford et al. 2013; Lewis et al. 2015) than expected based on where a galaxy with its stellar

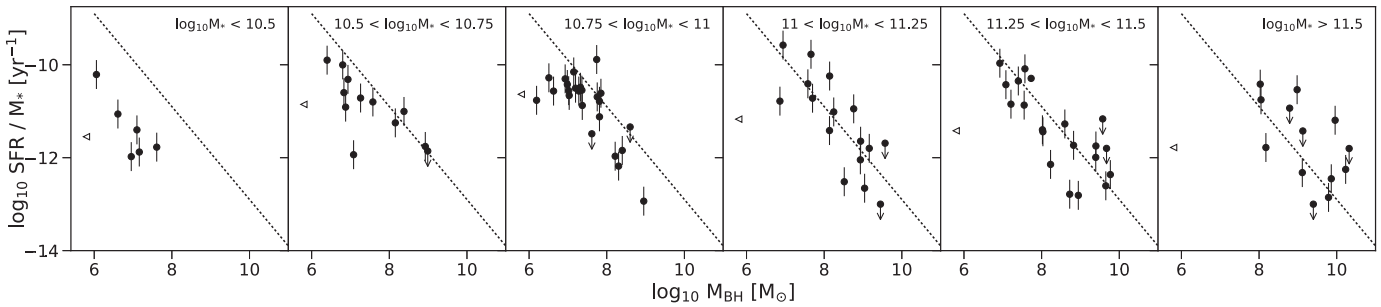

Figure 2. sSFR as a function of $M_{\rm BH}$ for different bins of M_*. The dotted lines are the same in each panel in order to compare the relations at high and low M_* bins. Open left-facing triangles indicate the median sSFR at each M_* bin.

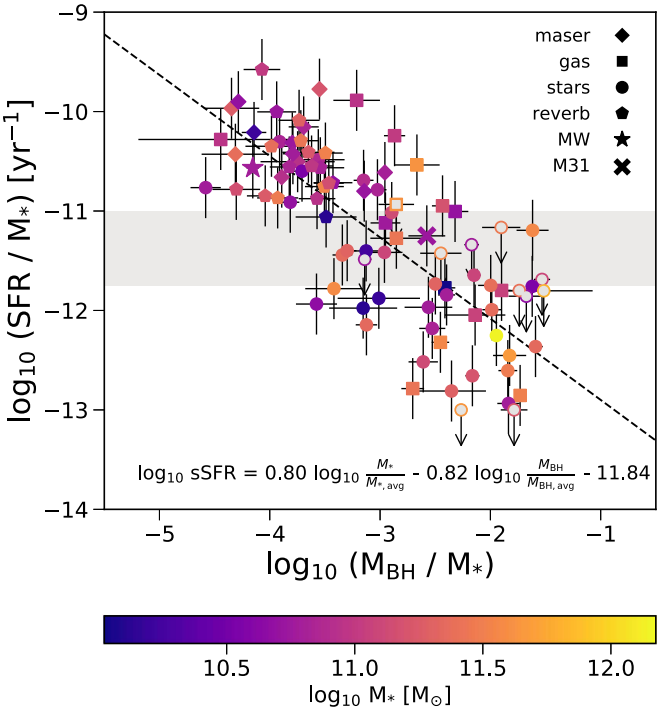

Figure 3. sSFR as a function of $M_{\rm BH}/M_*$ or $sM_{\rm BH}$ for our sample. The dashed line indicates the best-fit plane described by the equation shown at the bottom of the panel. Upper limits are not included in the fit and are indicated by open unfilled data points. The light gray shaded region highlights galaxies that are partially quiescent (see Section 4.2). The color gradient indicates M_*.

mass would be if it were on the star-forming main sequence. In our framework, this simply comes from the fact that M31 has an over-massive black hole for its stellar mass (i.e., a higher $sM_{\rm BH}$) and as a result gives us a lower sSFR. Similarly, M81 also lands within the partially quiescent sample and does not exhibit any morphological signs of transitioning.

If there are a significant number of stable galaxies with intermediate sSFRs, then this implies a more populated "green valley" than previously observed. In support of this implication, Oemler et al. (2017) argue that the "green valley" is more populated than is otherwise believed, which they base on the selection effects, systematic errors, and bias they find in one of the more popular collections of SFRs from SDSS (Brinchmann et al. 2004). They present a representative sample of local galaxies with updated and reliably measured SFRs from ultraviolet and mid-IR fluxes and find a significantly larger distinct population of galaxies with intermediate sSFRs. In addition, Eales et al. (2017) argue that the galaxy population exhibits a gradual difference in properties between star-forming and quiescent galaxies, a behavior that is erased in color-space because colors vary minimally below a threshold value of sSFR. This would challenge the widely accepted view that galaxies live in two distinct populations, and would instead argue for a more unitary approach. Finally, many studies have also argued for the existence of varying degrees of quiescence that could hint at a class of galaxies that spend an extended amount of time in the "green valley" (e.g., Lian et al. 2016; Pandya et al. 2016). Even so, our proposed framework of sSFR regulation by the black hole does not necessarily require a continuous distribution of galaxies along this relation since this distribution strongly depends on the details of black hole growth.

We note that our sample selection is biased and heterogeneous because we required a dynamical black hole mass measurement using a variety of detection methods. This affects our analysis in two ways. First, while we do not detect a significantly underpopulated "green valley" for the data in our sample, the current black hole data available are insufficient to probe the prominence of the "green valley" in the general central galaxy population since the sample is not representative. Future work will be important for determining the prominence of the "green valley" and the strength of bimodality in sSFR parameter space for central galaxies at this mass regime using reliable SFR indicators (see Oemler et al. 2017 and Eales et al. 2017 for important progress). Second, while it is clear that sSFR is a smoothly decreasing function of $sM_{\rm BH}$ for the current black hole data for central galaxies, we caution that the exact form of the relation may be affected by selection. For example, studies using the central stellar mass density within 1 kiloparsec ($\Sigma_{1\ \rm kpc}$) as an indirect proxy for $M_{\rm BH}$ see a relatively sudden drop in sSFR as a function of $\Sigma_{1\ \rm kpc}$ (Fang et al. 2013; Woo et al. 2015). We do not see evidence of this sudden drop in sSFR with our data set, perhaps because of the inadequacy of such proxies for $M_{\rm BH}$ or because of our sample size and inhomogeneities. It would be important to quantify the degree to which the dependence of sSFR is gradual and continuous with a larger and more complete sample, and to remain open to any higher order structure in the sSFR–$M_{\rm BH}$–M_* parameter space.

While we are proposing the possibility that much of the "green valley" population is in a quasi-stable state of partial quiescence, we also recognize that there likely exist various pathways a galaxy could take as it grows its black hole and stellar mass and varies its SFR. For example, rapid and more violent processes perhaps more common for giant ellipticals may skew the observed relationship between the sSFR, $M_{\rm BH}$, and M_*, as may be shown in the increased scatter in the relation

between $M_{\rm BH}$ and sSFR at high stellar masses. The existence of more than one quenching mode and speed has been discussed in other works (Martin et al. 2007; Barro et al. 2013; Schawinski et al. 2014; Woo et al. 2015; Lian et al. 2016). Whereas a quasi-stable state of partial quiescence would be consistent with slow quenching since the relevant timescales are comparable to or longer than a Hubble time, those experiencing faster quenching would likely account for some of the scatter between sSFR and $sM_{\rm BH}$. In addition, other processes that affect a galaxy's sSFR such as morphological quenching, stellar and supernovae Ia feedback, merging, or gravitational heating may affect a galaxy's position on the sSFR–$sM_{\rm BH}$ plane. Even so, the clear correlation between these three parameters shows that if our physical framework is at least generally valid, black hole feedback is the most important physical mechanism in determining a galaxy's star formation properties and that a large part of the galaxy sample can be characterized as being in a quasi-steady state or approaching this state as the sSFR responds to the change in $sM_{\rm BH}$ that the galaxy has undergone.

4.3. Model Comparison

Terrazas et al. (2016b) shows a strong correlation between $M_{\rm BH}$ and quiescence at a given stellar mass. When comparing these results to state-of-the-art models, they found that the latest Munich semi-analytic model (Henriques et al. 2015) and the Illustris hydrodynamic simulation (Vogelsberger et al. 2014) showed the best agreement with observations, unlike the EAGLE hydrodynamic simulation (Schaye et al. 2015) and GalICS semi-analytic model (Cattaneo et al. 2006). Here we focus on the Munich, Illustris, and EAGLE simulations since these explicitly use AGN feedback as the primary mechanism behind quiescence.

The Munich model includes a continuous heating rate affecting the temperature of the circumgalactic medium that depends on the hot halo gas mass and $M_{\rm BH}$. Illustris introduces buoyant bubbles that expand into the atmosphere every time the black hole is fed cold gas. While the creation of these bubbles is stochastic, the effect they have on the temperature of the circumgalactic medium is gradual as the bubble slowly expands into the gas. Hence, both of these models use either continuous or quasi-continuous heating from radio-mode AGN feedback in order to shut off star formation in galaxies at the high end of the stellar mass function. In contrast, EAGLE uses quasar-mode feedback to intermittently inject energy into the interstellar medium only when there is gas available to the black hole.

We find that the quantitative relationship between sSFR, $M_{\rm BH}$, and M_* vary from model to model. For example, at the stellar mass regimes of interest, the Munich model determination of a central galaxy's sSFR has little to no dependence on the stellar mass of the central galaxy and instead depends strongly on a $M_{\rm BH}$ threshold, see Terrazas et al. (2016a). Conversely, the sSFRs of Illustris depend more strongly on M_* such that more massive galaxies need more massive black holes in order to have the same sSFR as a lower mass galaxy, see Terrazas et al. (2016b). In Section 3 we fit a plane to our observational data that demonstrated that *in the real Universe,* the sSFR is a smoothly decreasing function of the ratio between $M_{\rm BH}$ and M_* (what we call the $sM_{\rm BH}$). However, in the Munich model, for example, a ratio of $M_{\rm BH}$ and $M_*^{0.1}$ would better reveal the physics behind quiescence since the Munich model

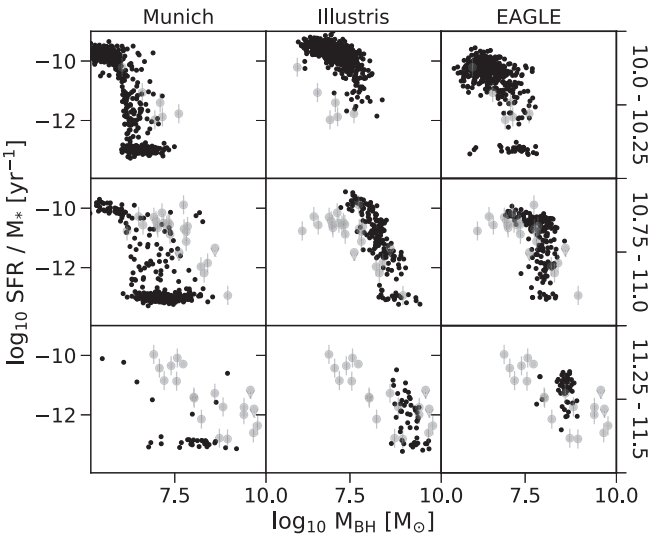

Figure 4. sSFR as a function of $M_{\rm BH}$ in three bins of M_* for the Munich, Illustris, and EAGLE galaxy formation models (black points). Overlaid are the observational data from Figure 2 in the corresponding M_* bins (gray translucent points). Each column indicates different models, and each row indicates the M_* bin: $10.25 < \log_{10} M_* < 10.5$ (top), $10.75 < \log_{10} M_* < 11.0$ (middle), and $11.25 < \log_{10} M_* < 11.5$ (bottom).

sSFRs barely depend on M_* and therefore require M_* to have a smaller power. As a result, the $sM_{\rm BH}$ will not be useful for understanding the suppression of sSFR in the models since they do not agree with observations in this respect.

Instead of introducing different powers of M_*, we choose to compare the models to our observational results by presenting the sSFR–$M_{\rm BH}$ plane at different M_* bins for each of these models. This effectively focuses on the dependence between the sSFR and $M_{\rm BH}$ instead of on the differences between M_* dependencies in the models. We show the distributions of these galaxies in Figure 4, where for each model we select only central galaxies within a 100 Mpc^3 volume at $z = 0$. The M_* bins are directly comparable to those in the first, third, and fifth panels of Figure 2, whose data points are overplotted in gray. Any galaxies with sSFR $< 10^{-13}$ yr^{-1} are assigned an arbitrarily low sSFR value defined by a normal distribution around this limit.

We find that the Munich model (left panels) exhibits a steep drop-off in sSFR at a given $M_{\rm BH}$ for most central galaxies. A clear bimodality exists where galaxies either have high or low sSFRs with a few galaxies in between. In the highest M_* bin there are very few galaxies, most of which have a massive black hole and therefore very low sSFR values. Terrazas et al. (2016a) show that most galaxies in this model are immediately quenched as soon as they reach a redshift-dependent critical $M_{\rm BH}$ (cee their Section 3 for more details).

The Illustris simulation (center panels) shows a considerably different distribution on this plane. Instead of showing a steep drop in specific SFR as a function of $M_{\rm BH}$ at a given M_*, it shows a smoothly declining function for galaxies with massive enough black holes to begin suppressing star formation, much like what is seen in our observational results in Figure 2. It is clear, however, that the black hole mass correlates more tightly with stellar mass in Illustris than in our observational sample since there there is a greater variety of black hole masses at each stellar mass bin in Figure 2 than for Illustris. In addition, galaxies with $M_{\rm BH} \lesssim 10^7\ M_\odot$ do not exhibit much dependence

on sM_{BH} since these galaxies' sSFRs are likely not regulated by AGN feedback in this model.

The EAGLE simulation (right panels) exhibits an L-shaped distribution where galaxies are mostly star-forming until they reach a certain M_{BH} value depending on their M_*, where many but not all galaxies begin to have lower sSFRs. As discussed in Terrazas et al. (2016b), this behavior is not reflected in the observation that star-forming and quiescent galaxies have distinct black hole mass distributions at a given M_*. The overlap in these distributions at high M_{BH} in this model likely arises because galaxies in EAGLE undergo intermittent heating episodes and not a continuous injection of energy. In this model, galaxies can continue forming stars once again in between feedback events even with a massive central black hole, producing an L-shaped distribution that is not reflected in our observational results. In other words, in EAGLE, a massive black hole is a necessary but not sufficient condition for quiescence in central galaxies since star-forming galaxies can also host massive black holes.

Each of these models have been quite successful in reproducing many of the observational trends out to $z = 2$, particularly the Munich model. Even so, it is clear that different physical implementations of quiescence can drastically affect the distributions in the sSFR–M_{BH}–M_* parameter space, even when they use similar physical frameworks for AGN feedback. As such, none of the models match our observational results perfectly, as is clear from the overlaid observational data (gray translucent points) in each panel. The models differ from each other and from the observations in this parameter space with respect to their variety of dependences on M_*, black hole mass distributions, stellar mass distributions, and strength of bimodality. This manifests itself as differences in the shape of the distributions, the slopes of the decline in sSFR, the normalization of the distributions in each M_* bin, and the scatter of sSFR as a function of M_{BH}.

However, qualitatively, we find that the results from Illustris better resemble our observational results. We note that the smoothly declining yet scattered relation between sSFR and M_{BH} in Illustris shows that even in an idealized simulation, an appreciable amount of scatter, such as what is seen in our observations, is expected within a framework where AGN feedback determines a galaxy's star formation properties.

Even so, it is well established that the AGN feedback in Illustris is too violent and ejects too much gas out of its hot halo (Vogelsberger et al. 2014). Further implementations of Illustris must be tested in order to understand whether this behavior persists with a less violent AGN feedback model. By extension, future models will need to consider how their prescriptions for AGN feedback correspond to the largely unexplored idea of a smoothly decreasing correlation between sSFR and sM_{BH} along with the idea of partial quiescence.

5. Conclusions

In order to more directly and statistically study AGN feedback in the context of galaxy relations, we choose to study the correlation between a galaxy's sSFR, M_{BH}, and M_*. We have shown that for our diverse sample of 91 central galaxies with dynamically detected M_{BH}, sSFR is a smoothly decreasing function of M_{BH}/M_*, or what we call the specific black hole mass, sM_{BH}. In an attempt to interpret this correlation, we propose a physical framework where the amount of gas heating from radio-mode AGN feedback is reflected by M_{BH} and diminishes the supply of fuel for star formation within the galaxy. In this framework, a galaxy with a more massive sM_{BH} would have a correspondingly lower sSFR, in accordance with our observational result.

This framework provides an alternative to the idea that all "green valley" galaxies are transitioning from star-forming to quiescent phases. Instead, it predicts that these galaxies with intermediate values of sM_{BH} live in a stable state of partial quiescence between star-forming and quiescent galaxies.

No current models achieve the distribution of galaxies that we see in this three-dimensional parameter space, although Illustris comes close. Future work will need to take these observational constraints into account when implementing AGN feedback models in order to shut off star formation in central galaxies.

B.A.T. is supported by the National Science Foundation Graduate Research Fellowship under Grant No. DGE1256260. We acknowledge helpful discussions with S. White, E. Gallo, J. Bregman, K. Gultekin, H. W. Rix, S. Faber, S. Ellison, A. Pontzen, L. Sales, B. O'Shea, M. Donahue, and M. Voit. This work used the SIMBAD database at CDS, and the NASA/IPAC Extragalactic Database (NED), operated by the Jet Propulsion Laboratory, California Institute of Technology, under contract with NASA.

References

Baldry, I. K., Glazebrook, K., Brinkmann, J., et al. 2004, ApJ, 600, 681
Balogh, M. L., Baldry, I. K., Nichol, R., et al. 2004, ApJL, 615, L101
Barro, G., Faber, S. M., Koo, D. C., et al. 2015, arXiv:1509.00469
Barro, G., Faber, S. M., Pérez-González, P. G., et al. 2013, ApJ, 765, 104
Behroozi, P. S., Conroy, C., & Wechsler, R. H. 2010, ApJ, 717, 379
Behroozi, P. S., Wechsler, R. H., & Conroy, C. 2013, ApJ, 770, 57
Bell, E. F. 2003, ApJ, 586, 794
Bell, E. F., van der Wel, A., Papovich, C., et al. 2012, ApJ, 753, 167
Bell, E. F., Wolf, C., Meisenheimer, K., et al. 2004, ApJ, 608, 752
Birnboim, Y., Dekel, A., & Neistein, E. 2007, MNRAS, 380, 339
Bîrzan, L., Rafferty, D. A., McNamara, B. R., Wise, M. W., & Nulsen, P. E. J. 2004, ApJ, 607, 800
Bluck, A. F. L., Mendel, J. T., Ellison, S. L., et al. 2014, MNRAS, 441, 599
Bower, R. G., Benson, A. J., Malbon, R., et al. 2006, MNRAS, 370, 645
Brammer, G. B., Whitaker, K. E., van Dokkum, P. G., et al. 2009, ApJL, 706, L173
Brinchmann, J., Charlot, S., White, S. D. M., et al. 2004, MNRAS, 351, 1151
Brown, M. J. I., Dey, A., Jannuzi, B. T., et al. 2007, ApJ, 654, 858
Cattaneo, A., Dekel, A., Devriendt, J., Guiderdoni, B., & Blaizot, J. 2006, MNRAS, 370, 1651
Cattaneo, A., Faber, S. M., Binney, J., et al. 2009, Natur, 460, 213
Cicone, C., Maiolino, R., Sturm, E., et al. 2014, A&A, 562, A21
Cisternas, M., Jahnke, K., Bongiorno, A., et al. 2011, ApJL, 741, L11
Croton, D. J., Springel, V., White, S. D. M., et al. 2006, MNRAS, 365, 11
Dale, D. A., Cohen, S. A., Johnson, L. C., et al. 2009, ApJ, 703, 517
David, L. P., Jones, C., Forman, W., et al. 2009, ApJ, 705, 624
Dekel, A., & Birnboim, Y. 2006, MNRAS, 368, 2
Dekel, A., Birnboim, Y., Engel, G., et al. 2009, Natur, 457, 451
Dekel, A., & Silk, J. 1986, ApJ, 303, 39
Di Matteo, T., Springel, V., & Hernquist, L. 2005, Natur, 433, 604
Eales, S., de Vis, P., W. L. Smith, M., et al. 2017, MNRAS, 465, 3125
Engelbracht, C. W., Rieke, G. H., Gordon, K. D., et al. 2008, ApJ, 685, 678
Faber, S. M., Willmer, C. N. A., Wolf, C., et al. 2007, ApJ, 665, 265
Fabian, A. C. 2012, ARA&A, 50, 455
Fang, J. J., Faber, S. M., Koo, D. C., & Dekel, A. 2013, ApJ, 776, 63
Ford, G. P., Gear, W. K., Smith, M. W. L., et al. 2013, ApJ, 769, 55
Franx, M., van Dokkum, P. G., Förster Schreiber, N. M., et al. 2008, ApJ, 688, 770
Gabor, J. M., & Davé, R. 2015, MNRAS, 447, 374
Gaspari, M., Brighenti, F., D'Ercole, A., & Melioli, C. 2011, MNRAS, 415, 1549
Ghosh, S. K., Bisht, R. S., Iyengar, K. V. K., et al. 1992, ApJ, 391, 111

Gitti, M., O'Sullivan, E., Giacintucci, S., et al. 2010, ApJ, 714, 758
Gonçalves, T. S., Martin, D. C., Menéndez-Delmestre, K., Wyder, T. K., & Koekemoer, A. 2012, ApJ, 759, 67
Guo, Q., White, S., Li, C., & Boylan-Kolchin, M. 2010, MNRAS, 404, 1111
Henriques, B. M. B., White, S. D. M., Thomas, P. A., et al. 2015, MNRAS, 451, 2663
Hopkins, P. F., Quataert, E., & Murray, N. 2012, MNRAS, 421, 3522
Huchra, J. P., Macri, L. M., Masters, K. L., et al. 2012, ApJS, 199, 26
Ilbert, O., McCracken, H. J., Le Fèvre, O., et al. 2013, A&A, 556, A55
Jarrett, T. H., Chester, T., Cutri, R., Schneider, S. E., & Huchra, J. P. 2003, AJ, 125, 525
Johansson, P. H., Naab, T., & Ostriker, J. P. 2009, ApJL, 697, L38
Kang, Y., Bianchi, L., & Rey, S.-C. 2009, ApJ, 703, 614
Kauffmann, G., & Haehnelt, M. 2000, MNRAS, 311, 576
Kauffmann, G., Heckman, T. M., White, S. D. M., et al. 2003, MNRAS, 341, 33
Kennicutt, R. C., & Evans, N. J. 2012, ARA&A, 50, 531
Knapp, G. R., Guhathakurta, P., Kim, D.-W., & Jura, M. A. 1989, ApJS, 70, 329
Kormendy, J., & Ho, L. C. 2013, ARA&A, 51, 511
Kormendy, J., & Kennicutt, R. C., Jr. 2004, ARA&A, 42, 603
Krause, E., Hirata, C. M., Martin, C., Neill, J. D., & Wyder, T. K. 2013, MNRAS, 428, 2548
Landt, H., Buchanan, C. L., & Barmby, P. 2010, MNRAS, 408, 1982
Lang, P., Wuyts, S., Somerville, R. S., et al. 2014, ApJ, 788, 11
Lewis, A. R., Dolphin, A. E., Dalcanton, J. J., et al. 2015, ApJ, 805, 183
Lian, J., Yan, R., Zhang, K., & Kong, X. 2016, ApJ, 832, 29
Madau, P., & Dickinson, M. 2014, ARA&A, 52, 415
Mandelbaum, R., Wang, W., Zu, Y., et al. 2016, MNRAS, 457, 3200
Martig, M., Bournaud, F., Teyssier, R., & Dekel, A. 2009, ApJ, 707, 250
Martin, D. C., Wyder, T. K., Schiminovich, D., et al. 2007, ApJS, 173, 342
Mendez, A. J., Coil, A. L., Lotz, J., et al. 2011, ApJ, 736, 110
Mortlock, A., Conselice, C. J., Hartley, W. G., et al. 2015, MNRAS, 447, 2
Moshir, M., et al. 1990, BAAS, 22, 1325
Moster, B. P., Somerville, R. S., Maulbetsch, C., et al. 2010, ApJ, 710, 903
Muzzin, A., Marchesini, D., Stefanon, M., et al. 2013, ApJ, 777, 18
Oemler, A., Jr, Abramson, L. E., Gladders, M. D., et al. 2017, ApJ, 844, 45
Pan, Z., Li, J., Lin, W., Wang, J., & Kong, X. 2014, ApJL, 792, L4
Pandya, V., Brennan, R., Somerville, R. S., et al. 2016, arXiv:1611.03869
Peng, Y.-j., Lilly, S. J., Kovač, K., et al. 2010, ApJ, 721, 193
Porter, L. A., Somerville, R. S., Primack, J. R., & Johansson, P. H. 2014, MNRAS, 444, 942
Reines, A. E., Greene, J. E., & Geha, M. 2013, ApJ, 775, 116
Rice, W., Lonsdale, C. J., Soifer, B. T., et al. 1988, ApJS, 68, 91
Saglia, R. P., Opitsch, M., Erwin, P., et al. 2016, ApJ, 818, 47
Salim, S., Rich, R. M., Charlot, S., et al. 2007, ApJS, 173, 267
Schawinski, K., Urry, C. M., Simmons, B. D., et al. 2014, MNRAS, 440, 889
Schaye, J., Crain, R. A., Bower, R. G., et al. 2015, MNRAS, 446, 521
Serjeant, S., & Hatziminaoglou, E. 2009, MNRAS, 397, 265
Shang, Z., Brotherton, M. S., Wills, B. J., et al. 2011, ApJS, 196, 2
Shin, J., Woo, J.-H., & Mulchaey, J. S. 2016, ApJS, 227, 31
Sijacki, D., Springel, V., Di Matteo, T., & Hernquist, L. 2007, MNRAS, 380, 877
Sijacki, D., Vogelsberger, M., Genel, S., et al. 2015, MNRAS, 452, 575
Surace, J. A., Sanders, D. B., & Mazzarella, J. M. 2004, AJ, 127, 3235
Taylor, E. N., Hopkins, A. M., Baldry, I. K., et al. 2015, MNRAS, 446, 2144
Temi, P., Brighenti, F., & Mathews, W. G. 2009, ApJ, 707, 890
Tempel, E., Tamm, A., & Tenjes, P. 2010, A&A, 509, A91
Terrazas, B. A., Bell, E. F., Henriques, B. M. B., et al. 2016b, ApJL, 830, L12
Terrazas, B. A., Bell, E. F., Henriques, B. M. B., & White, S. D. M. 2016a, MNRAS, 459, 1929
Tomczak, A. R., Quadri, R. F., Tran, K.-V. H., et al. 2014, ApJ, 783, 85
van den Bosch, R. 2016, ApJ, 831, 134
Vogelsberger, M., Genel, S., Springel, V., et al. 2014, MNRAS, 444, 1518
Wetzel, A. R., Tinker, J. L., & Conroy, C. 2012, MNRAS, 424, 232
White, S. D. M., & Frenk, C. S. 1991, ApJ, 379, 52
White, S. D. M., & Rees, M. J. 1978, MNRAS, 183, 341
Woo, J., Dekel, A., Faber, S. M., & Koo, D. C. 2015, MNRAS, 448, 237